JOURNAL OF PHYSICAL ORGANIC CHEMISTRY, VOL. 8, 407–420 (1995)

AB INITIO MOLECULAR ORBITAL STUDY OF THE O + C_6H_5O REACTION

M. C. LIN AND A. M. MEBEL
Department of Chemistry, Emory University, Atlanta, Georgia 30322, U.S.A.

An *ab initio* molecular orbital study of the potential energy surface of the $C_6H_5O + O$ reaction was performed at the PUMP3/6–31G*//UHF/6–31G* + ZPE(UHF/6–31G*) level of theory. Various reaction channels were considered. The most favorable mechanisms, Ia and Ib, start from the attachment of the oxygen atom to the carbon atom of the C_6 ring in the *ortho-* or *para* position with respect to CO, taking place without activation energy. Then, either hydrogen elimination by mechanism Ia or 1,2-H shift from the C(H)(O) group takes place; the latter process leads to the formation of the very stable $C_6H_4(O)(OH)$ radical, which can also eliminate H by mechanism Ib. Thus, the main products of the C_6H_5O ($^2B_1$) + O(^3P) reaction are *o/p*-benzoquinones and the hydrogen atom. At low temperatures, however, the system may be trapped in the potential well of the $C_6H_4(O)(OH)$ intermediate. At high temperatures, the reaction may proceed by the formation and decomposition of *o/p*-benzoquinones. Because of their higher activation energies, the reaction mechanisms giving rise to other products – the attachment of the oxygen atom to the bridging position to form an epoxy intermediate, followed by insertion of O into the CC bond and dissociation to give C_5H_5 and CO_2 (channel IIc), in addition to the attachment of oxygen to the terminal O atom of C_6H_5O followed by elimination of O_2 (channel III) – cannot compete with channel Ia or Ib. RRKM calculation was carried out for the total and individual rate constants for channels Ia and Ib. The three-parameter expression for the total rate constant, fitted by the least-squares method for the temperature range of 300–3000 K, is given as $k_{tot} = 5{\cdot}52 \times 10^{-17}\, T^{1{\cdot}38}\, e^{+148/T}$ cm^3 mol^{-1} s^{-1}.

INTRODUCTION

The phenoxy radical is an important reactive intermediate in the oxidation of small aromatic hydrocarbons, key additives to lead-free gasoline.[1,2] The C_6H_5O radical may be produced by several processes, for example

$$C_6H_5 + O_2 \rightarrow C_6H_5O + O$$
$$O + C_6H_5CH_3 \rightarrow C_6H_5O + CH_3$$
$$C_6H_6 + OH \rightarrow C_6H_5OH + H \rightarrow C_6H_5O + 2H$$

On account of the relatively high stability of the C_6H_5O radical in comparison with those of alkoxy radicals, it may undergo extensive bimolecular reactions with reactive combustion species such as O atoms, in addition to its well known unimolecular fragmentation process:[2–5]

$$C_6H_5O \rightarrow C_5H_5 + CO$$

The bimolecular O + C_6H_5O association reaction is not only very exothermic but also is expected to be fast because it is a radical–radical association process. On account of the presence of resonance structures in C_6H_5O, viz.

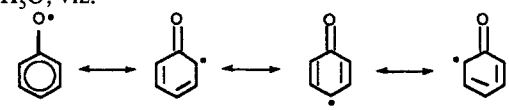

the O + C_6H_5O reaction may take place via several pathways. In order to elucidate the mechanism of this important reaction, we have carried out a detailed calculation using various *ab initio* molecular orbital techniques for the intermediates and also the transition states of major reaction paths associated with the O + C_6H_5O and C_6H_5OO systems.

In this paper, the energetics and structures of the major intermediates and transition states derived from the association process are presented. The rate constants for some of the reaction steps were calculated on the basis of the RRKM theory.

As discussed in the following section, we used the UHF approach for geometry optimization and perturbation theory methods for the refinement of energies. However, for several structures considered, particularly the transition states, the wavefunctions might not have a single dominant configuration in the CI expansion.

CCC 0894–3230/95/060407–14

Received 9 December 1994
Revised 3 February 1995

Thus, for these structures, the perturbation theory methods which take into account only dynamic electron correlation and do not include non-dynamic correlation, are not expected to be accurate enough and the results should be considered with caution. More sophisticated techniques, such as CASPTN or MRCI, would provide better geometries and energetics, but these methods are extremely expensive for systems of such size as $C_6H_5O + O$. The approach we used is the only one feasible now. Although our calculations provide only semi-quantitative energetics for various transition states and intermediates, they offer a valuable guide for the $C_6H_5O + O$ reaction potential energy surface and possible reaction mechanisms. In order to obtain quantitative data, more extensive calculations at higher levels of theory would be necessary.

CALCULATION PROCEDURE

We employed the same calculation methods as we used before in the study of various geometric isomers of $C_6H_5O_2$.[6] The geometries of different intermediates and transition states were optimized at the UHF/6–31G* level. Vibrational frequencies have been calculated at the same level of theory for characterization of the nature of stationary points, for zero-point energy corrections and to obtain vibrational frequencies. All the calculated transition states have one and the intermediates have zero imaginary frequencies. We expect the geometric parameters obtained at the UHF level to be of semi-quantitative accuracy, and more accurate geometries may be achieved with the use of the methods which take electron correlation into account. The UHF wavefunction can be subject to serious spin contamination (see $\langle S^2 \rangle$ values before projection in Table 1), which may lead to artificially low relative energies for the structures having large deviations of $\langle S^2 \rangle$ from the correct value (0·75 for doublets). More reliable energies of various structures have been obtained by the UMP4(SDQ)/6–31G* method at the UHF optimized geometries. The spin-projected PUMP2 and PUMP3 energies are expected to be more accurate than the energies by the regular UMP2, UMP3 and UMP4 (SDQ) methods. Hence, we consider the PUMP3/6–31G*//UHF/6–31G* + ZPE (UHF/6–31G*) level of calculation as the highest one in the present study. The calculated ZPE were scaled by 0·893 to account for anharmonicity.[7] The calculations were performed by using the GAUSSIAN 92 program.[8]

RESULTS AND DISCUSSION

We consider the following potential reaction mechanisms:

(i) Oxygen atom attacks a carbon atom of the ring to form a $C_6H_4O(O)(H)$ isomer of the $C_6H_5O_2$ radical. It was shown earlier[6] that *ortho* and *para* configurations of $C_6H_4O(O)(H)$ can exist. Accordingly, the attack of O can occur at either the *ortho* or *para* position with respect to the C═O group of the phenoxy radical. On the other hand, *o*- and *p*-$C_6H_4O(O)(H)$ radicals have similar electronic structures and energies. Therefore, we expect potential energy surfaces for the $C_6H_5O + O \rightarrow o\text{-}C_6H_4O(O)(H) \rightarrow \ldots$ and $C_6H_5O + O \rightarrow p\text{-}C_6H_5O(O)H \rightarrow \ldots$ reaction mechanisms to resemble each other. Therefore, we performed the calculations only for one of these channels involving the formation of $o\text{-}C_6H_4O(O)(H)$.

(ii) Oxygen approaches the C atom connected to the O atom in C_6H_5O.

(iii) The O atom attacks the terminal oxygen of the phenoxy radical to form a phenyl peroxy radical, C_6H_5OO.

The structures of reactants, products, intermediates and transition states for the reaction are shown in Figure 1 and their energies at different levels of theory are presented in Table 1. Various reaction mechanisms are illustrated in Figures 2–7, and the overall potential energy surface is drawn in Figure 8.

Mechanism Ia: hydrogen atom elimination after oxygen atom addition

The transition state for oxygen addition to a carbon in the *ortho*-position relative to C═O is the structure **1**. The barrier, calculated at the UHF/6–31G* + ZPE level, is 12·7 kcal mol^{-1} (1 kcal = 4·184 kJ). However, taking electron correlation into account significantly reduces the energy of the transition structure (TS) **1**. At our best PUMP3/6–31G* + ZPE level, **1** is 8·7 kcal mol^{-1} lower than the reactants. Obviously, the UHF/6–31G* optimized geometry of the transition state is not accurate enough. The wavefunction for TS **1** probably has a multi-reference character which is indicated by the high spin contamination (see $\langle S^2 \rangle$ value in Table 1). In order to obtain a more accurate barrier height, the use of a multi-configuration method for geometry optimization and the use of the MRCI or the restricted open-shell coupled cluster methods for the energy calculation would be necessary. On the basis of our PUMP3//UHF/6–31G* calculations, we conclude here that the barrier for oxygen addition is very low, if it exists.

The addition of the O atom to C_6H_5O gives the *o*-$C_6H_4O(O)(H)$ radical **2**, which lies 33·2 kcal mol^{-1} below the reactants at the PUMP3//UHF/6–31G* + ZPE level. The geometry of **2** was discussed earlier.[6] Let it only be mentioned here that the carbon ring in **2** contains two single CC bonds, C^1C^2 and C^2C^3 (1·51–1·53 Å), two double bonds, C^3C^4 and C^5C^6 (1·36–1·38 Å) and two CC bonds of an intermediate length, (1·44–1·46 Å). The C^1O bond is double (1·21 Å), the C^2O is single (1·39 Å), and the unpaired electron is located on the oxygen atom of the $C^2(H)(O)$ fragment. In the reactant,

Table 1. Total and relative energies of various intermediates and transition states of the C_6H_5O + O reaction

Species	$\langle S^2\rangle$[a]	ZPE[b]	E[c] HF	UMP4 (SDQ)	PUMP3
$C_6H_5O + O$	1·39	53·6 (0)	−379·75897 [0·0]	−380·77683 [0·0]	−380·78366 [0·0]
o-$C_6H_4O_2$ + H	0·0	51·6 (0)	−379·71959 [22·7]	−380·84514 [−44·9]	−380·82604 [−28·6]
p-$C_6H_4O_2$ + H	0·0	51·6 (0)	−379·73380 [13·8]	−380·85673 [−52·1]	−380·83824 [−36·2]
$C_6H_5 + O_2$	1·43	53·6 (0)	−379·68298 [47·7]	−380·74558 [19·6]	−380·74920 [21·6]
TS **1**, C_1	2·19	54·1 (1)	−379·73955 [12·7]	−380·78308 [−3·4]	−380·79829 [−8·7]
o-$C_6H_4O(O)(H)$ (**2**), C_1	1·57	55·9 (0)	−379·76972 [−4·4]	−380·83645 [−35·1]	−380·84017 [−33·2]
TS **3**, C_1	2·06	53·8 (1)	−379·72723 [20·1]	−380·78969 [−7·9]	−380·80300 [−11·9]
TS **4**, C_1	1·67	52·6 (1)	−379·71585 [26·1]	−380·80542 [−18·9]	−380·81433 [−20·2]
TS **5** $^2A'$, C_s	1·00	54·0 (1)	−379·69832 [38·5]	−380·82207 [−28·0]	−380·81547 [−19·6]
o-$C_6H_4O(OH)$ (**6**), $^2A''$,C_s	1·31	56·8 (0)	−379·83541 [−44·8]	−380·92820 [−91·8]	−380·93107 [−89·3]
TS **7**, $^2A''$, C_s	2·28	49·6 (1)	−379·70191 [31·8]	−380·75694[8·5]	−380·76600 [7·0]
TS **7'**, C_1	2·08	50·1 (1)	−379·73340 [12·5]	−380·79588 [−15·5]	−380·81140 [−20·9]
TS **8**, C_1	2·27	53·8 (1)	−379·71328 [28·9]	−380·75384 [14·6]	−380·75836 [16·1]
o-$C_6H_4O(O)_{br}$ (**9**), C_1	0·78	57·8 (0)	−379·73012 [22·3]	−380·84657 [−39·6]	−380·83398 [−27·4]
TS **10**, C_1	1·90	54·4 (1)	−379·71373 [29·2]	−380·78338 [−3·3]	−380·79303 [−5·1]
$C_6H_5O(O)$ (**11**), C_1	2·23	54·4 (0)	−379·72488 [22·2]	−380·76499 [8·2]	−380·77050 [9·0]
$C_6H_5(O_2)$ (**12**), $^2B_1$, C_{2v}	1·21	55·7 (0)	−379·68706 [47·2]	−380·79813 [−11·3]	−380·79623 [−5·8]
TS **13**, C_1	1·59	54·8 (1)	−379·72917 [19·9]	−380·81926 [−25·4]	−380·82557 [−25·1]
TS **14**, C_1	1·37	55·3 (1)	−379·70457 [35·9]	−380·79921 [−12·2]	−380·79951 [−8·3]
C_6OH_5O (**15**), $^2A''$, C_s	1·25	56·5 (0)	−379·80828 [−28·0]	−380·90205 [−75·7]	−380·90015 [−70·2]
TS **16**, $^2A''$, C_s	1·68	54·5 (1)	−379·70688 [33·6]	−380·78380 [−3·5]	−380·79260 [−4·7]
C_6H_5OO (**17**), $^2A''$, C_s	0·77	57·7 (0)	−379·71539 [31·4]	−380·83436 [−32·0]	−380·82109 [−19·4]
C_6H_5OO (**17'**), $^2A''$, C_s	0·76	57·7 (1)	−379·71299 [33·0]	−380·83063 [−29·7]	−380·81727 [−17·0]
TS **18**, $^2A''$, C_s	1·38	54·8 (1)	−379·67244 [55·5]	−380·77884 [2·5]	−380·78354 [1·3]

[a] $\langle S^2\rangle$ value before projection. Values after projection are 0·75 for doublets.
[b] ZPE are calculated at the UHF/6–31G* level and scaled by 0·893. In parentheses: number of imaginary frequencies.

the phenoxy radical, the single electron is situated in the π electronic system of the ring and is distributed among all carbon atoms and the terminal oxygen atom. The C^1C^2 and C^1C^6 bonds, 1·44 Å, are longer than the other CC bonds. The CO bond in C_6H_5O is slightly elongated with respect to a regular C=O. According to the geometry, **1** is an early TS. The CO distance for the forming bond in **1** is 0·45 Å longer than that in **1**. Geometric parameters of the ring for **1** are intermediate between those for C_6H_5O and **2**, but somewhat closer to the geometry of the reactant. The early character of the transition state **1** is in accord with exothermicity of the oxygen addition. Because electron correlation increases the exothermicity, we expect that reoptimization at the UMP2/6–31G* level would render the TS **1** earlier and looser, with a longer C^2O distance. The activation energy calculated at the PUMP3//UHF/6–31G* level is negative because the UHF geometry of **1** is closer to that of the product **2** than the geometry corresponding to the transition state at the correlation level.

The $C_6H_4O(O)(H)$ radical **2** can eliminate the hydrogen atom connected to C^2 via transition state **3**. The barrier is calculated to be 21·3 kcal mol^{-1} relative to **2**, and **3** lies 11·9 kcal mol^{-1} below the reactants at the PUMP3//UHF/6–31G* + ZPE level. The hydrogen elimination leads to *o*-benzoquinone, $C_6H_4O_2$. The products, $C_6H_4O_2$ + H, are 4·6 kcal mol^{-1} higher than **2** and 28·6 kcal mol^{-1} lower than the reactants. It is difficult to characterize the transition state **3** as early or late, because geometric parameters of the ring in **3** are not exactly between those in **2** and $C_6H_4O_2$, although the deviations are small. The C^2H distance in **3** for the breaking bond is 0·62 Å longer than that in **2**, the C^2O distance in the transition state is 0·11 Å shorter than that in **3**, but 0·09 Å longer than C^2O double bond length in benzoquinone. We expect that reoptimization at the UMP2 level should render the C^2H distance in **3** shorter and make the TS earlier because of smaller endothermicity of the process when electron correlation is taken into account. Note that the barrier for the reverse reaction of hydrogen atom addition to o-benzoquinone is calculated to be 16·7 kcal mol^{-1}.

The reaction channel $C_6H_5O + O \rightarrow \mathbf{1} \rightarrow \mathbf{2} \rightarrow \mathbf{3} \rightarrow$ *o*-$C_6H_4O_2$ + H is exothermic and, at high temperatures, may be followed by the unimolecular decomposition of *o*-benzoquinone. Therefore, the mechanism of this decomposition is worth studying by *ab initio* methods in the future.

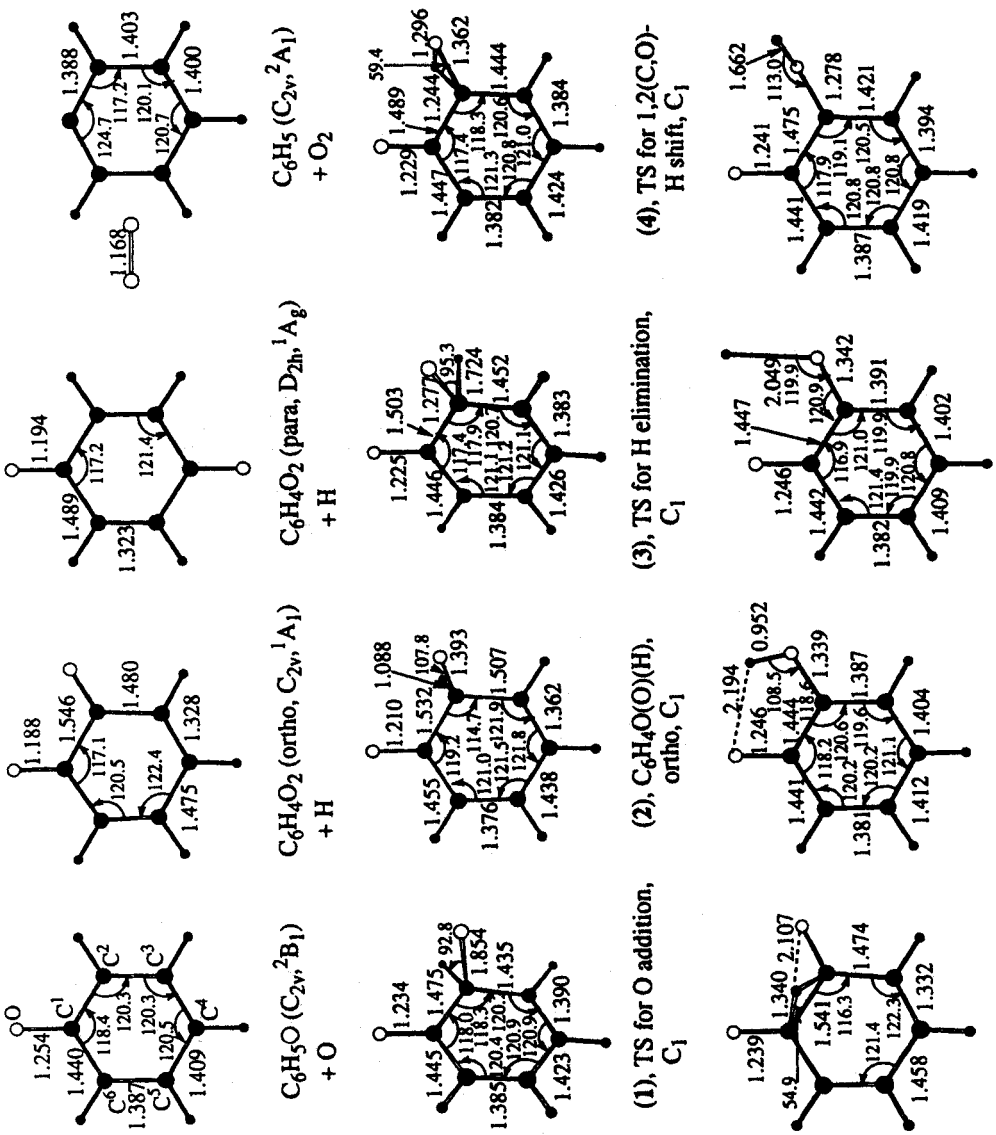
C6H5O (C2v, 2B1) + O
C6H4O2 (ortho, C2v, 1A1) + H
C6H4O2 (para, D2h, 1Ag) + H
C6H5 (C2v, 2A1) + O2
(1), TS for O addition, C1
(2), C6H4O(O)H, ortho, C1
(3), TS for H elimination, C1
(4), TS for 1,2(C,O)-H shift, C1
(5), TS for 1,2(C,C)-H shift, Cs, 2A'
(6), C6H4O(OH), ortho, Cs, 2A"
(7), TS for H elimination, Cs, 2A"
(7'), TS for H elimination, C1

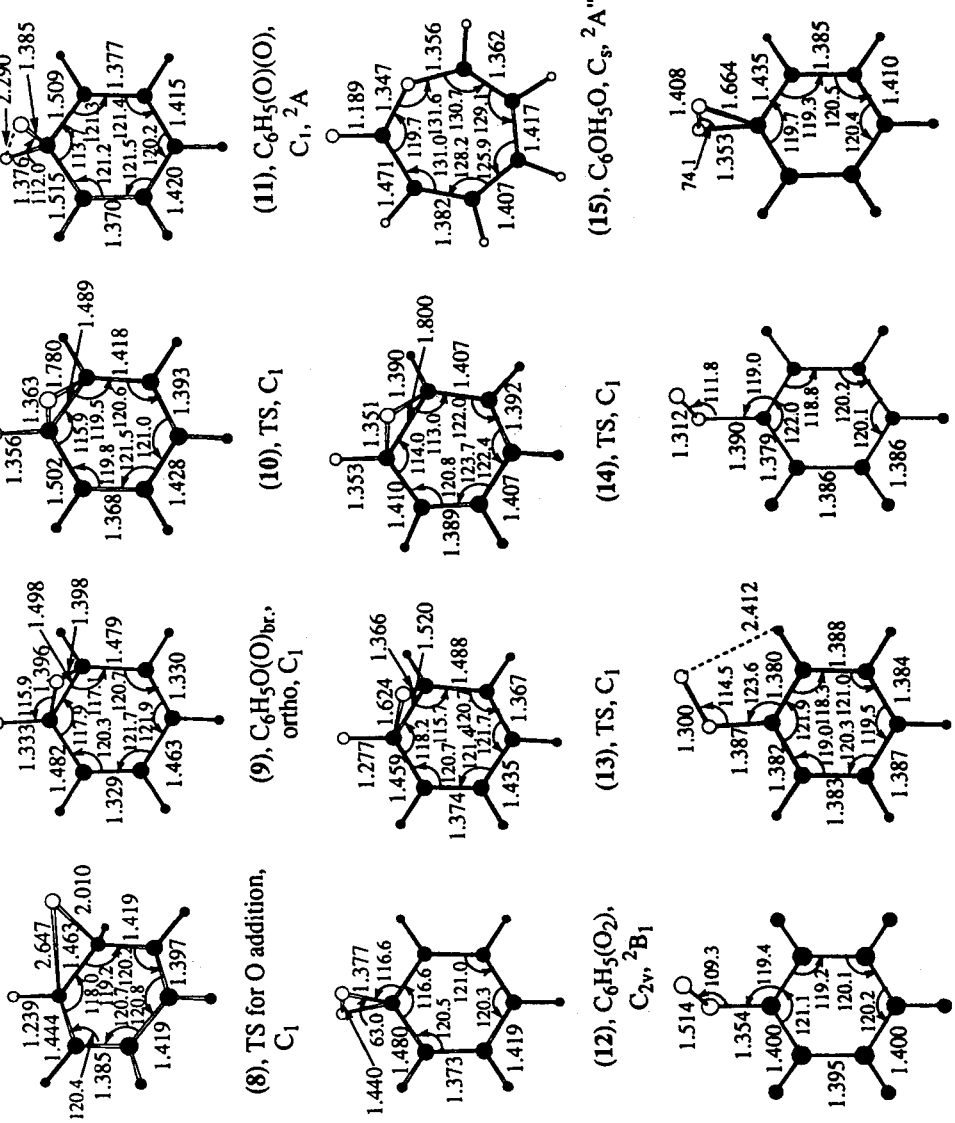

Figure 1. UHF/6–31G* optimized geometries of various intermediates and transition states of the C_6H_5O + O reaction.

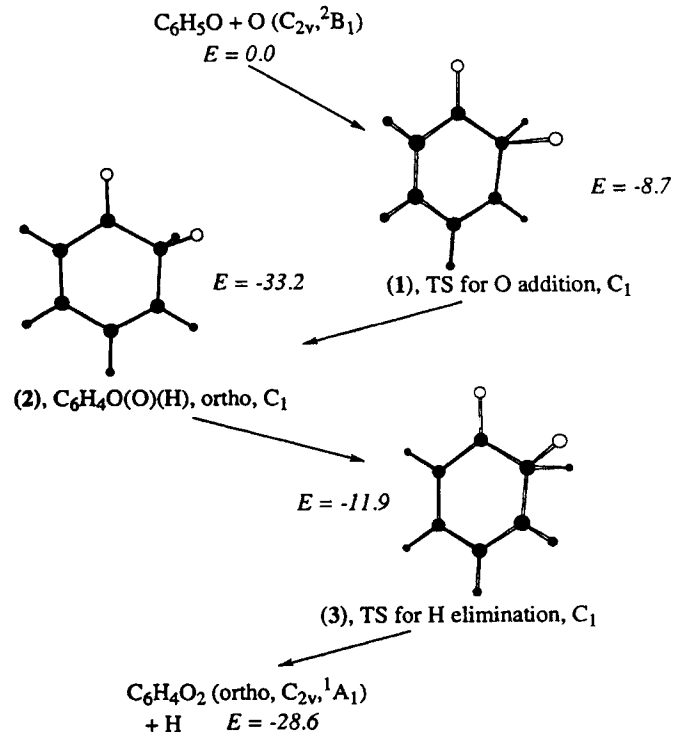

Figure 2. Mechanism Ia of the $C_6H_5O + O$ reaction

Mechanism Ib: hydrogen migration after oxygen addition

After the intermediate **2** is formed, the migration of the hydrogen atom attached to the C^2 atom can take place. It has been shown that the *o*-hydroxylphenoxy, $C_6H_4O(OH)$, is the most stable isomer of the $C_6H_5O_2$ species.[6] In principle, *o*-$C_6H_4O(OH)$ (**6**) can be formed by either 1,2- or 1,3-hydrogen shift in $C_6H_4O(O)(H)$ (**2**). Therefore, we have performed the optimization of transition states for two different kinds of hydrogen migration. The structure **4** is the transition state for the 1,2-H shift from C^2 to the oxygen atom connected with C^2. The three atoms, C^2, H and O, in **4** form a three-membered ring; C^2H is elongated only by 0·15 Å relative to that in *2*, while the OH distance in **4** is 0·34 Å longer than that in **6**. In this case, **4** is an early transition state, in accord with high exothermicity of the process (56·1 kcal mol^{-1}). The barrier for the 1,2-H shift is not high, 13 kcal mol^{-1} at the PUMP3/6–31G* + ZPE level, and the transition state **4** lies 20·2 kcal mol^{-1} below the reactants.

We also tried to find the transition state for the 1,3-hydrogen migration from C^2 to the oxygen atom connected with C^1. The hydrogen shift is a sigmatropic reaction in which a σ-bonded entity, the atom H, migrates from one terminus of a π-system to the other. While the 1,2-H shift is an allowed sigmatropic rearrangement for suprafacial geometry, the 1,3-hydrogen migration is symmetry forbidden.[9,10] This explains why we were unable to locate the transition state for the 1,3-H shift. In the initial geometry, which we used to start the transition state search, the migrating H atom was located at a similar distance between C^2 and the O-atom connected to C^1. However, the optimization converged to the structure **5**, where the hydrogen atom is connected with C^2 and C^1 and occupies a bridging position between them; **5** is actually a transition state for the 1,2-H shift from one carbon atom to the other and corresponds to the degenerated **2**→**2** rearrangement. Thus, our *ab initio* calculations confirm the validity of simple selection rules based on the orbital symmetry consideration. However, the 1,3-H shift can occur in a stepwise manner, 1,2(C,C)—H shift followed by 1,2(C,O) shift leading to the 1,3(C,O)—H migration. The transition state **5** lies 19·6 kcal mol^{-1} below $C_6H_5O + O$, only 0·6 kcal mol^{-1} higher than **4**. The barrier for the **2**→**2** reorganization is 13·6 kcal mol^{-1} with respect to **2**. Structure **5** has C_s symmetry with the mirror plane containing the critical H atom and perpendicular to the plane of the ring. The bridged CC distance is lengthened to 1·54 Å. Also, in the ring there

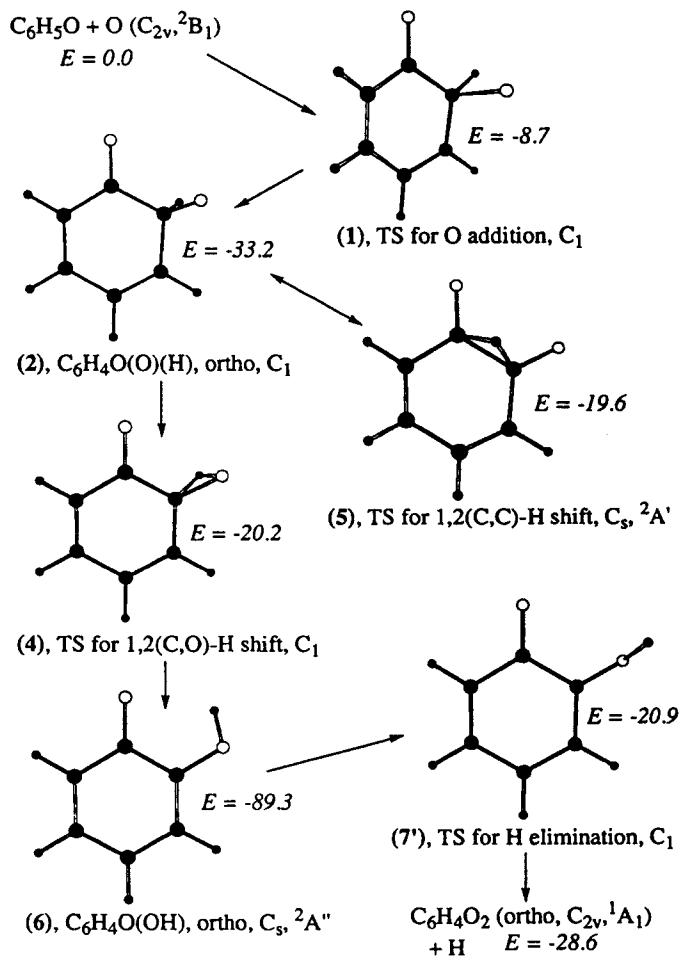

Figure 3. Mechanism Ib of the C_6H_5O + O reaction.

are three single CC bonds (1·46–1·47 Å) and two double bonds (1·33 Å).

After the formation of the stable isomer **6** by hydrogen migration in **2**, the system can, in principle, eliminate the hydrogen atom of the hydroxyl group, creating *o*-$C_6H_4O_2$. This dissociation reaction is endothermic by 60·7 kcal mol^{-1} We have located two separate transition states for the hydrogen elimination. The TS **7** is planar, and the corresponding barrier is high, 96·3 kcal mol^{-1} relative to **6** and 7·0 kcal mol^{-1} above the reactants. The reverse process, a hydrogen atom addition to the *o*-benzoquinone then requires 35·6 kcal mol^{-1}. The origin of this high barrier is that during the *o*-$C_6H_4O_2 \rightarrow C_6H_4O(OH)$ reaction, the π C^2O bond has to be broken, and the σ OH bond is formed. Therefore, the planar geometry is not advantageous for the transition state. Indeed, optimization without symmetry constraints gives another transition state, **7'**, with much lower energy. The barrier for hydrogen elimination from **6** through TS **7'** is 68·4 kcal mol^{-1}, 20·9 kcal mol^{-1} below the reactants. The reverse barrier is only 7·7 kcal mol^{-1}, 9 kcal mol^{-1} lower than the barrier for the *o*-$C_6H_4O_2 + H \rightarrow$ **3** $\rightarrow C_6H_4O(O)(H)$ (**2**) reaction. Also, the barrier **7'** is very close to the barrier for the reverse hydrogen migration, **6** $\rightarrow$ **4** $\rightarrow$ **2**. Moreover, the transition state **7'** is much looser than **4**, and the entropy factor makes the reverse hydrogen migration less probable than the hydrogen elimination to form benzoquinone, as will be discussed later. TS **7'** is an earlier transition state than **7** relative to the reactant **6**; it has a significantly shorter OH distance, 1·66 Å vs. 2·05 Å in **7**. Whereas the $C_6H_4O_2$ fragment remains planar in **7'**, the breaking OH bond is perpendicular to this plane.

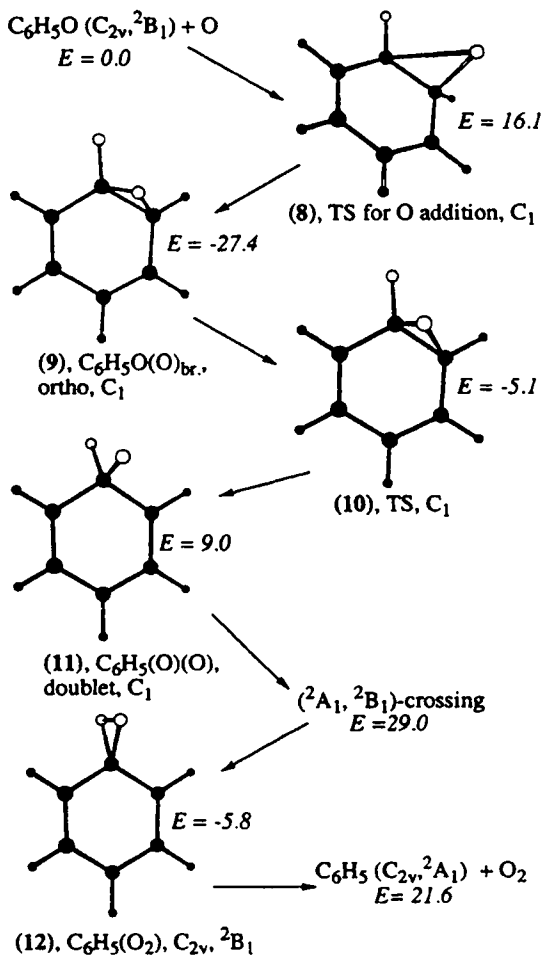

Figure 4. Mechanism IIa of the $C_6H_5O + O$ reaction.

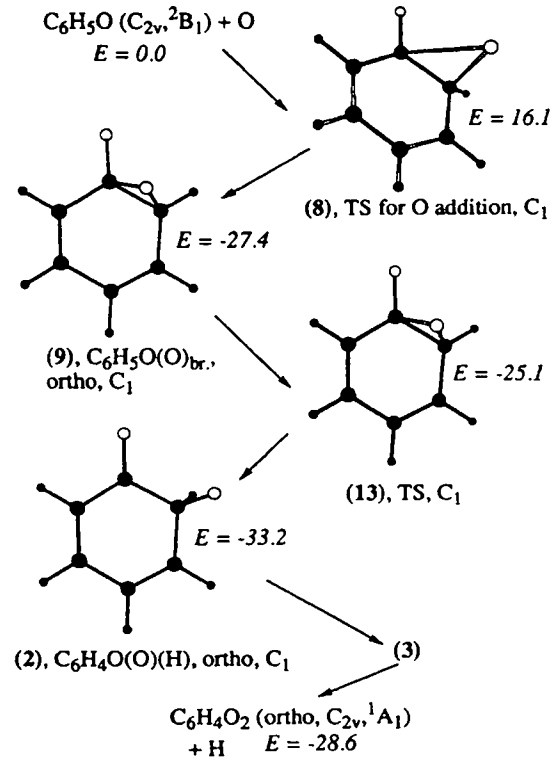

Figure 5. Mechanism IIb of the $C_6H_5O + O$ reaction.

It is necessary to mention here that at the UHF/6–31G* level the energies of the transition states 7′ and 3 are lower than the energy of the *o*-$C_6H_4O_2$ + H product (see Table 1). This means that some association complex, $C_6HO_2 \cdot H$, exists at this level of theory. However, the existence of the complex is not relevant for the reaction kinetics and may be artifact of the UHF approximation, because at higher levels, with electron correlation taken into account, 7′ and 3 lie higher than *o*-$C_6H_4O_2$ + H.

Mechanism IIa: Oxygen addition to a bridging position, migration and O_2 elimination

At the beginning, our calculations were targeted to locate a transition state for oxygen atom addition to the C^1 atom forming the $C_6H_5(O)(O)$ isomer. Hence we started the saddle point search from the geometry close to that of **11**, but with an elongated critical CO distance. The optimization converged to the structure **8**. The C^1O distance in **8**, 2·65 Å, is longer than the C^2O distance, 2·01 Å. Therefore, it is more favorable for the oxygen atom to attack C_6H_5O from the C^2 side than from the C^1 side. The transition structure **8** connects $C_6H_5O + O$ with the ortho *epoxy*-isomer **9**, but not with **11**. The barrier at the transition state **8** is 16·1 kcal mol^{-1} with respect to the reactants. The $C_6H_5O + O \rightarrow 8 \rightarrow 9$ reaction is exothermic by 27·4 kcal mol^{-1}.

The epoxy isomer **9** formed after the oxygen addition can be transformed in three different ways: oxygen migration to the left or right and oxygen insertion into the C^1C^2 bond. Mechanism IIa involves the migration of the O atom from the bridging position to C^1. The structure $C_6H_5(O)O$ (**11**) is formed as a result of this oxygen shift; **11** lies 9·0 kcal mol^{-1} above the $C_6H_5O + O$ system, and the endothermicity of the $9 \rightarrow 11$ isomerization is 36·4 kcal mol^{-1}. The transition state search between **9** and **11**, carried out at the UHF/6–31G* level, led to the structure **10**.

In the UHF/6–31G* approximation, **10** is 7 kcal mol^{-1} higher than **11** and has one imaginary frequency corresponding to the oxygen migration.

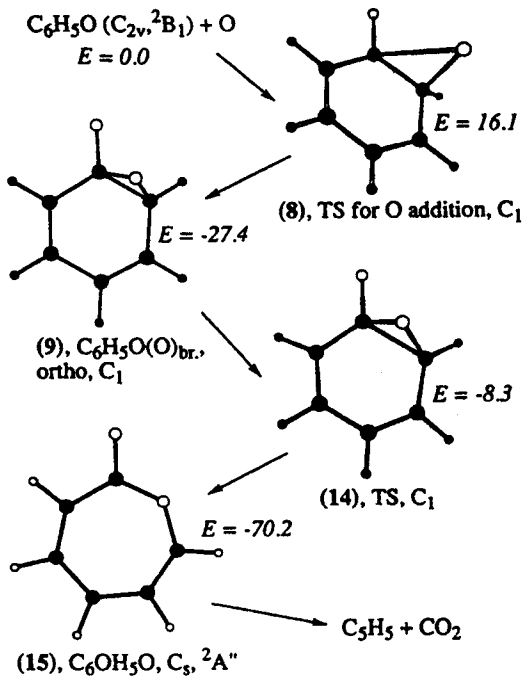

Figure 6. Mechanism IIc of the C_6H_5O + O reaction.

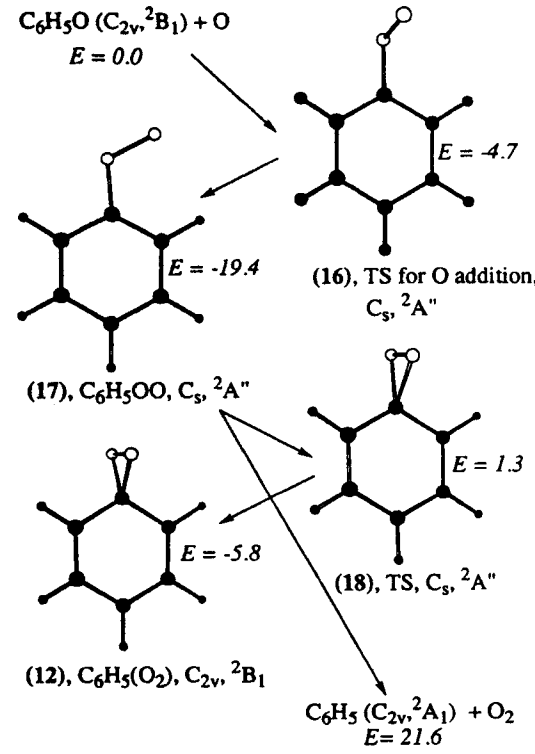

Figure 7. Mechanism III of the C_6H_5O + O reaction.

However, at the higher PUMP3/6–31G* + ZPE level theory, the transition state **10** becomes lower than the isomer **11** by 14·1 kcal mol^{-1}. This means that the geometry of **10** would significantly change if a higher level of theory such as MP2/6–31G* were employed for optimization. According to the increase of the **9**→**11** endothermicity from 3·3 kcal mol^{-1} at the UHF/6–31G to 36·4 kcal mol^{-1} at the PUMP3/6–31G* + ZPE level, the geometry of **10** would become much closer to that of **11** with the electron correlation taken into account, increasing the late character of the TS. The conclusion is that the isomer **11**, if it exists, is separated by a small barrier from **9**.

The structure **11** can rearrange to the π-complex $C_6H_5(O_2)$ (**12**). The π-complex has C_{2v} symmetry with two O atoms and the C-atom C^1, forming an almost equilateral triangle perpendicular to the C_6 plane. The ground electronic state of **12** is $^2B_1$, and the unpaired electron is spread out between the C atoms and involved in the π electronic system of the ring. Although the $C_6H_5(O)O$ structure **11** has no symmetry, it is very close by geometry and energy to the symmetric C_{2v} structure with $^2A_1$ electronic state. We attempted to locate a barrier between **11** and **12**, searching for a transition state without symmetry constraints, but could not locate the saddle point at the UHF level. The reason may be that the wavefunction in the transition-state vicinity has a multi-reference character, including contributions of the electronic states of $^2B_1$ and $^2A_1$ origin in the C_{2v} symmetry, and it (wavefunction) cannot be described properly by the single reference HF method. In order to estimate the upper limit of the barrier between **11** and **12**, we have calculated the seam of crossing between $^2A_1$ and $^2B_1$ potential energy surfaces within the C_{2v} symmetry. Geometries of the C_6 rings and the CO bond lengths in **11** and **12** are very similar; the greatest difference in the interatomic distances is only 0·02 Å. The only geometric parameter changing in the transformation is the OCO angle, 112° in **11** and 63° in **12**. Therefore, we looked for the crossing point by varying this angle, while for other geometric parameters we took the values' average between **11** and **12** and did not change them. The calculations of energy of the $^2A_1$ and $^2B_1$ electronic states at different values of OCO were carried out at the PUMP3/6–31* level of theory. We located the crossing point at the OCO angle value of 94·266°, and the energy difference between the two states, which characterizes the accuracy of our calculations, is only 0·038 kcal mol^{-1}. The real seam of crossing might lie slightly lower, but the difference is expected to be negligible because of the small geometric difference

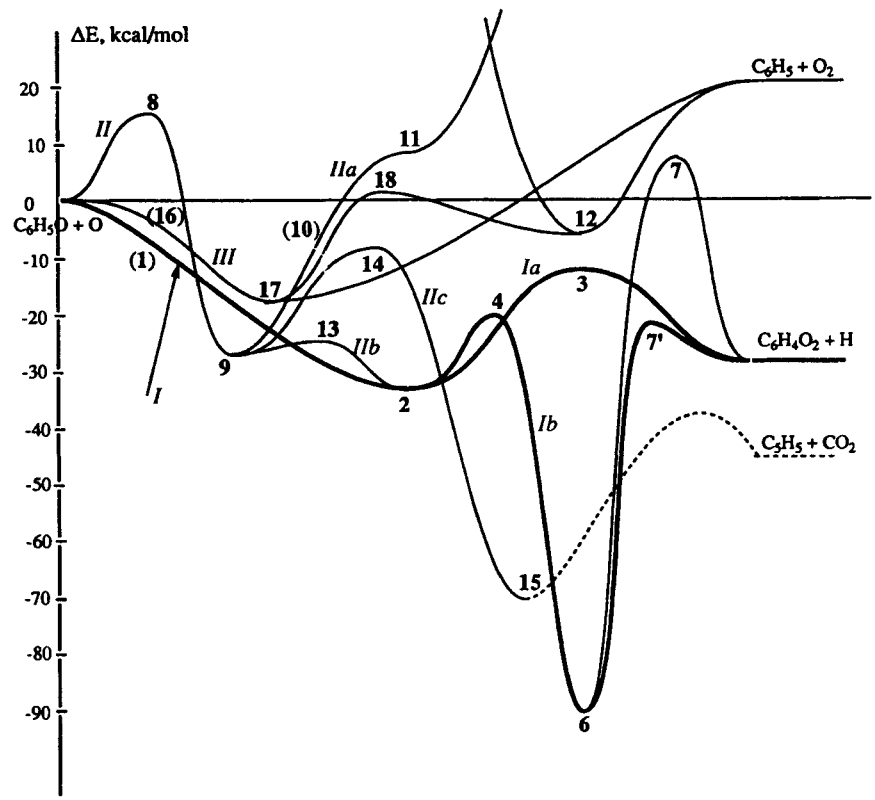

Figure 8. Overall profile of potential energy surface for the $C_6H_5O + O$ reaction, calculated at the PUMP3/6–31G*//UHF/6–31G* + ZPE (UHF/6–31G*) level.

between **11** and **12**. The crossing point is 20·0 kcal mol^{-1} higher than **11** and 29·0 kcal mol^{-1} higher than the reactants at the PUMP3/6–31G* + ZPE level, if we use the zero-point energy of **11** as an estimate of ZPE for the crossing point structure. The $C_6H_5(O)O \rightarrow C_6H_5(O_2)$ transformation can occur via conical intersection with a breaking of the C_{2v} symmetry. Therefore, the activation energy for the process is expected to be lower than 29·0 kcal mol^{-1} relative to $C_6H_5O + O$.

The final step of this mechanism is the elimination of molecular oxygen from the π-complex **12**. It occurs without any barrier leading to $C_6H_5 + O_2$, and the endothermicity of this step is 27·4 kcal mol^{-1}. The overall endothermicity of the $C_6H_5O + O \rightarrow C_6H_5 + O_2$ reaction at the PUMP3//UHF/6–31G* level is 21·6 kcal mol^{-1}. The calculations significantly overestimate the experimental value of 8 kcal mol^{-1}.[11] The $C_6H_5(O)O \rightarrow C_6H_5(O_2)$ transformation is the rate-controlling step for the mechanism IIa, and the calculated energy is high. Hence this mechanism is not expected to compete effectively with the mechanisms Ia and Ib.

Mechanism IIb: oxygen addition to a bridging position, migration and H elimination

The branching of the mechanism II starts from the epoxy isomer $C_6H_5O(O)_{br}$ (**9**). The (b) subchannel involves the oxygen migration from the bridging position in the right-hand direction to form the *o*-$C_6H_4O(O)(H)$ isomer **2**. A transition state between **9** and **2** is the structure **13**. The barrier for the oxygen shift is not high, only 2·3 kcal mol^{-1} relative to **9**, and **13** lies 25·1 kcal mol^{-1} lower than the reactants. In the TS, the oxygen atom is shifted slightly closer to C^2, the C^2O distance is shortened by 0·03 Å with respect to that in **9** and the C^1O distance is elongated by 0·22 Å. The geometry and bonding character in the carbon ring do not change much during the transformations. The $9 \rightarrow 13 \rightarrow 2$ reaction step is exothermic by 5·8 kcal mol^{-1}, and the transition state **13** is early.

From the structure **2**, mechanism IIb merges with mechanism I, and the reaction proceeds either by hydrogen atom elimination or the formation of $C_6H_4O(OH)$. The rate-determining step for IIb is oxygen addition to

the bridging position, with the transition state structure *8* and an activation energy of 16·1 kcal mol^{-1}. Therefore, this mechanism is less favorable than Ia or Ib but is significantly more favorable than IIa.

Mechanism IIc: oxygen atom insertion into CC bond

The third option for the system transformation starting from the structure **9** is insertion of the bridging oxygen into the C^1C^2 bond. As a result, the seven-membered ring isomer, $C_6O(H)_5O$ (**15**) is formed; **15** is 42·8 kcal mol^{-1} more stable than **2** and lies 70·2 kcal mol^{-1} below $C_6H_5O + O$. $C_6O(H)_5O$ has a planar geometry and $^2A'$ ground electronic state. The unpaired electron is distributed between the carbon atoms of the ring, excluding C^1, at the π MO. The CO bonds in the ring have a single bond character (1·35–1·36 Å), whereas the out-of-ring CO bond is a regular double bond (1·19 Å). The structure **14** corresponds to a transition state between **9** and **15**. The breaking C^1C^2 bond length in **14** is 0·30 Å longer than that in **9**, while the bridging C^1O and C^2O distances remain nearly unchanged. The barrier for the oxygen insertion is high enough, 19·1 kcal mol^{-1} relative to **9**, but the transition structure **14** is still 8·3 kcal mol^{-1} lower than the reactants. Similarly to IIb, the rate-controlling step for mechanism IIc is the initial oxygen addition with the barrier of 16·1 kcal mol^{-1}. Recently, Carpenter[12] suggested, on the basis of semi-empirical PM3 calculations, that the seven-membered ring structure **15** is an important intermediate for the reaction of phenyl radical with molecular oxygen. However, according to our data, that is not the case. Once the *o*-epoxy intermediate **9** is formed, oxygen migration to C^2 producing **2** with a barrier of 2·3 kcal mol^{-1} is much more favorable than insertion into the CC bond (the barrier is 19·1 kcal mol^{-1}). Carpenter[12] has shown that $C_6O(H)_5O$ (**15**) can decompose, giving the cyclopentadienyl radical C_6H_5 and CO_2. We do not consider this channel in the present paper, but it deserves to be studied in the future. Note that for the $C_6H_5O + O$ reaction, mechanism IIc is not competitive with Ia and Ib, or even with IIb.

Mechanism III: oxygen atom addition to the terminal oxygen of the phenoxy radical and elimination of O_2

At the first step of the mechanism III, the O atom attaches the terminal oxygen of C_6H_5O, forming the phenylperoxy radical, C_6H_5OO (**17**). The latter is shown to be the initial intermediate of the $C_6H_5 + O_2$ reaction. As we discuss;ed earlier,[6] the ground electronic state of the $C_6H_5O + O$ system is $^2A'$ if the oxygen atom at infinite distance remains in the molecule plane, while the electronic state of C_6H_5OO is $^2A''$. Therefore, the $C_6H_5O + O \rightarrow C_6H_5OO$ association reaction occurs with a break of symmetry, via a non-planar transition state, if the latter exists. The saddle-point search without symmetry constraints leads to the TS **16**, which has a plane of symmetry perpendicular to the C_6 ring plane and containing the forming COO group. The transition state is late and tight; the OO distance, 1·51 Å, is only about 0·2 Å longer than that in the C_6H_5OO intermediate. During the association process, the CO double bond is broken and a new OO single bond is formed. The barrier at the UHF level is high. However, at the PUMP3/6–31G* + ZPE level the energy of TS **16** is 4·7 kcal mol^{-1} lower than the energy of $C_6H_5O + O$. Owing to the reaction exothermicity at the correlated levels, we expect that the structure of **16** becomes looser with reoptimization at the MPn level of theory. The association barrier, if it exists, is expected to be low. Meanwhile, the energy of TS **16** is noticeably higher than the energy of TS **1**, and the structure of **16** is significantly tighter than that of **1**. Hence the addition of the oxygen atom to the ring is preferable to the addition to the terminal oxygen of C_6H_5O.

C_6H_5OO (**17**) has a planar geometry, and the structure **17'** with the COO plane perpendicular to the C_6 plane has one imaginary frequency and corresponds to the transition state of OO rotation around the CO single bond. The geometric parameters of **17'** are close to those of **17**, and the rotational barrier is low, 2·4 kcal mol^{-1} at the PUMP3/6–31G* + ZPE level. The process of C_6H_5O and O association, therefore, involves the approach of the oxygen atom in the plane perpendicular to the ring and then the rotation of the OO bond after clearing of a bifurcation point, when the OO distance decreases.

The phenylperoxy radical can directly eliminate the O_2 molecule without any barrier, with a calculated endoergicity of 41·0 kcal mol^{-1}, which is in good agreement with the experimental estimate of 37 kcal mol^{-1}.[13] On the other hand, **17** can be transformed into the π-complex **12**, which is 13·6 kcal mol^{-1} higher in energy. Structure **18** is the transition state for this rearrangement. The barrier is 20·7 kcal mol^{-1} relative to **17**, and **18** lies 1·3 kcal mol^{-1} higher than $C_6H_5O + O$. The **17** $\rightarrow$ **12** reaction is endothermic, and the transition state **18** has a late character with geometry close to that of the π-complex. The O_2 fragment is moved from the plane of the C_6 ring on the perpendicular one. The symmetry of **18** is C_s, as is that of **17**, but the mirror plane is perpendicular to the ring. The COO angle changes from 114·5° in **17** to 74·1° in **18** and 58·5 in **12**. The OO distance in the transition state is 0·11 Å longer than that in C_6H_5OO and only 0·03 Å shorter than this bond length in π-$C_6H_5(O_2)$.

The π-complex **12** can also dissociate to $C_6H_5 + O_2$. On the other hand, it can be transformed into $C_6H_5(O)O$ (**11**) via the conical intersection of the ($^2A_1$, $^2B_1$) seam of crossing, and then to the *o*-epoxy intermediate **9**. This branch of the present channel merges with the mechanism II.

Hence, the mechanism III, $C_6H_5O + O \rightarrow C_6H_5OO \rightarrow C_6H_5 + O_2$, has the elimination of molecular oxygen as the rate-controlling step. This channel of the reaction seems to be too endothermic to compete effectively with mechanisms Ia and Ib.

RRKM calculation for the main channels of the reaction

RRKM calculation was carried out for the total and individual rate constants for the channels Ia and Ib shown by the bold curves in Figure 8. For the individual channel rate constants we used our earlier equations[14-16] and a multi-channel computer program previously written for the $CH_3 + O_2$ reaction.[16]

For a multi-channel reaction A + B which occurs via a long-lived intermediate AB:

$$A + B \underset{b}{\overset{a}{\rightleftharpoons}} AB^{\dagger} \xrightarrow{c} C + D$$

$$\xrightarrow{d} E + F$$

$$\xrightarrow[[M]]{e} AB$$

the rate constants for the disappearance of the reactant A or B into various products, including the stabilization process (e), can be evaluated as follows:[16]

$$k_i = I_a \frac{kT}{h} \frac{Q_t^{\#} Q_r^{\#}}{Q_A Q_B} e^{-E_a/RT} \int_0^{\infty} \frac{k_{E_i} \Sigma P(E^{\#}) e^{-E^{\#}/RT}}{\Sigma_i k_{E_i} + \omega} \frac{dE^{\#}}{RT} \quad (1)$$

$$k_e = I_a \frac{kT}{h} \frac{Q_t^{\#} Q_r^{\#}}{Q_A Q_B} e^{-E_a/RT} \int_0^{\infty} \frac{\omega \Sigma P(E^{\#}) e^{-E^{\#}/RT}}{\Sigma_i k_{E_i} + \omega} \frac{dE^{\#}}{RT} \quad (2)$$

where i = b, c and d and I_a is the reaction path degeneracy for the formation of $AB^{\dagger}$, the chemically activated vibrationally excited intermediate, via step (a); Q_A and Q_B are total partition functions of A and B, respectively; $Q_t^{\#}$ and $Q_r^{\#}$ are the translational and rotational partition functions of the transition state $AB^{\#}$ for step (a), which has an energy barrier E_a at 0 K. In the integrals, ω is the effective collision frequency for the deactivation of $AB^{\dagger}$ by step (e), calculated on the basis of Troe's weak collision treatment,[17] and

$$k_{E_i} = C_i \Sigma P_i(E_i^{\#})/hN(E) \quad (3)$$

are the specific rate constants for the decomposition of $AB^{\dagger}$ by steps (b), (c) and (d). In equation (3), C_i is the product of statistical factor and the ratio of the overall rotational partition function of the transition state and the AB adduct for the unimolecular reaction step (i); $\Sigma P_i(E_i^{\#})$ is the sum of states of the transition state for step (i) with energy $E_i^{\#}$; $N(E)$ is the density of states of $AB^{\dagger}$ having a total energy E; i = b, c and d. In the case of the $C_6H_5O + O$ reaction, A is C_6H_5O and B is the O atom, AB is the *o*-$C_6H_4O(O)(H)$ intermediate **2**, C + D is *o*-$C_6H_4O_2 + H$, and E + F is $C_6H_4O(OH)$ **6**. The transition state for step (a) or reverse step (b) is **1**; the transition states for steps (c) and (d) are TS **3** and **4**, respectively. The total rate constant for the disappearance of C_6H_5O is:

$$k_{tot} = k_c + k_d + k_e$$

The molecular parameters of various active species involved in mechanisms Ia and Ib, including the transition states, are summarized in Table 2. The activation energy for the initial reaction step, $C_6H_5O + O \rightarrow C_6H_4O(O)(H)$ (**2**), is assumed to be zero, while the other energetic parameters were taken from the PMP3 relative energies (Table 1). The Arrhenius plots of the rate constants calculated at 760 Torr Argon pressure (1 Torr = 133·3 Pa) in the temperature range 300–3000 K are shown in Figure 9.

One can see that channel Ib, $C_6H_5O + O \rightarrow$ *o*-$C_6H_4O(OH)$ (**6**) (k_d) dominates the reaction at the temperatures up to 2500 K, when it becomes competitive with channel Ia, $C_6H_5O + O \rightarrow$ *o*-$C_6H_4O_2 + H$ (k_c). The rate constant k_e for the stabilization process, $C_6H_5O + O \rightarrow C_6H_4O(O)(H)$ (**2**), is always lower than k_d because TS **4** lies much lower than the reactants and most of the excited adduct molecules pass through this barrier rather than be stabilized to the intermediate **2**. k_e decreases rapidly with rising temperature and becomes lower than k_c at $T > 700$ K. The total reaction rate constant exhibits a positive temperature dependence because it is controlled by channel Ib, having an activation energy of 13·0 kcal mol^{-1}, but not by the recombination process.

The three-parameter expressions for the total rate constant, k_{tot}, and k_d, fitted by the least-squares method for the temperature range 300–3000 K, can be given in cm^3 mol^{-1} s^{-1} units by

$$k_{tot} = 5{\cdot}52 \times 10^{-17} T^{1{\cdot}38} e^{148/T}$$

$$k_d = 4{\cdot}30 \times 10^{-14} T^{0{\cdot}47} e^{-400/T}$$

CONCLUSIONS

Several different channels have been studied for the reaction of C_6H_5O ($^2B_1$) with O (^3P). The most favorable mechanisms, Ia and Ib, start from the attachment of the oxygen atom to the carbon C^2 in the *ortho* position with respect to the CO bond of C_6H_5O. The association takes place without activation energy. Then, either hydrogen elimination (mechanism Ia) or 1,2-H

Table 2. Molecular and transition-state parameters used in the RRKM calculations

Species or transition state	i	I_i (10^{-40} g cm^2)	ν_j (cm^{-1})
C_6H_5O	A	152·8	191, 350, 427, 449, 485,
C_6H_6	B	302·2	558, 607, 715, 744, 765
	C	455·0	831, 894, 909, 922, 945,
			1013, 1087, 1106, 1247, 1262,
			1276, 1392, 1399, 1458, 1464,
			3000, 3011, 3020, 3030, 3032
TS 1	A	293·0	97, 181 (2), 348, 481(4),
	B	370·5	873 (12), 1353 (7),
	C	556·9	3020 (5), 545i
o-$C_6H_4O(O)(H)$ (2)	A	272·5	43, 194, 261, 378, 439, 449,
	B	348·0	501, 535, 642, 690, 717, 785,
	C	581·2	871, 900, 905, 917, 966, 1056
			1081, 1120, 1196, 1271, 1310,
			1369, 1394, 1413, 1495, 2855,
			3004, 3015, 3026, 3034
TS 3	A	259·9	108, 231, 322, 461 (5),
	B	356·7	753 (10), 1263 (10)
	C	603·9	3024 (4), 922i
TS 4	A	258·0	115, 270 (2), 533 (8),
	B	361·9	952 (6), 1261 (10), 2027,
	C	615·0	3022 (4), 2050i

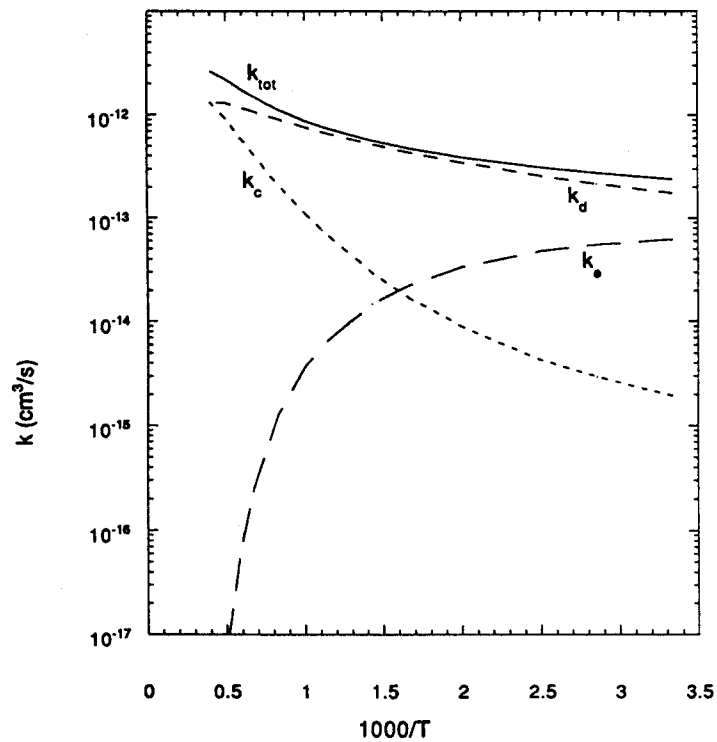

Figure 9. Arrhenius plots of rate constants from the RRKM calculation for the processes of $C_6H_5O + O \rightarrow o\text{-}C_6H_4O_2 + H$ (k_c, channel Ia), $C_6H_5O + O \rightarrow o\text{-}C_6H_4O(OH)$ (k_d, channel Ib), and $C_6H_5O + O \rightarrow o\text{-}C_6H_4O(O)(H)$ (k_e, stabilization of **2**), at 760 Torr pressure; $k_{tot} = k_c + k_d + k_e$. The molecular parameters used in the RRKM calculation are presented in Table 2. The activation energy for formation of **2** from C_6H_5O and O via TS **1** is assumed to be zero; the other energetic parameters were taken from the relative energies at the PUMP3 level (Table 1). The average step size used in the calculation with Troe's weak-collision approximation[17] is $-\langle\Delta E\rangle = 1$ kcal mol^{-1}.

shift from the $C^2(H)(O)$ group take place; the latter process leads to the formation of the very stable $C_6H_5O(OH)$ radical **6**, which can eliminate H by mechanism Ib. Both mechanisms produce *o*-benzoquinone and a hydrogen atom. Of other reaction mechanisms, only IIb is expected to be possible at high temperatures. It is initiated by oxygen addition to the bridging position with the formation of the *o*-epoxy intermediate **9**, proceeds by the O-atom migration to C^2 and is completed by the hydrogen atom elimination. The rate-determining step is the initial step with an activation energy of 16·1 kcal mol^{-1}. Channel IIc involving oxygen insertion into the CC bond with formation of the seven-membered ring intermediate **14** cannot compete with IIb because the insertion barrier is much higher than the barrier for O shift. Mechanisms IIa and III producing $C_6H_5 + O_2$ cannot compete with other channels owing to their high activation energies.

We also expect that the channel with oxygen addition to the *p*-C atom of the ring to form *p*-$C_6H_5O(O)(H)$ would have the energetics and other parameters similar to those of mechanism Ia. Thus, the main products of the C_6H_5O $(^2B_1) + O(^3P)$ reaction are *o*/*p*-benzoquinones and hydrogen atoms. At low temperatures, the system may be trapped in the potential well of the very stable $C_6H_4(O)(OH)$ intermediate **6**. At high temperatures, the reaction would proceed by the formation and decomposition of the *o*/*p*-benzoquinones.

ACKNOWLEDGMENTS

The authors gratefully acknowledge the support of this work by the Division of Chemical Sciences, Office of Energy Sciences, DOE (contract no. DE-FGO5-91 ER14192). They also thank the Cherry L. Emerson Center for Scientific Computation for the use of the computing facilities and various programs. Helpful discussion with Dr E. W. Diau on RRKM calculations is greatly appreciated.

REFERENCES

1. I. Glassman, *Combustion*, 2nd ed. Academic Press, New York (1986).
2. K. Brezinsky, *Prog. Energy Combust. Sci.* **12**, 1 (1986).
3. A. J. Colussi, F. Zabel and S. W. Benson, *Int. J. Chem. Kinet.* **9**, 161 (1977).
4. C.-Y. Lin and M. C. Lin, *J. Phys. Chem.* **20**, 425 (1986).
5. A.-M. Schmoltner, D. S. Anex and Y. T. Lee, *J. Phys. Chem.* **96**, 1236 (1992).
6. A. M. Mebel and M. C. Lin, *J. Am. Chem. Soc.* **116**, 9577 (1994).
7. W. Hehre, L. Radom, P. v. R. Schleyer and J. A. Pople, *Ab Initio Molecular Orbital Theory*. Wiley, New York (1986).
8. M. J. Frisch, G. W. Trucks, M. Head-Gordon, P. M. W. Gill, M. W. Wong, J. B. Foresman, B. G. Johnson, H. B. Schlegel, M. A. Robb, E. S. Replogle, R. Gomperts, J. L. Andres, K. Raghavachari, J. S. Binkley, C. Gonzales, R. L. Martin, D. J. Fox, D. J. DeFrees, J. Baker, J. J. P. Stewart and J. A. Pople, *GAUSSIAN 92*. Gaussian, Pittsburgh (1992).
9. N. S. Isaacs, *Physical Organic Chemistry*. Wiley, New York, 1987.
10. (a) R. B. Woodward and R. Hoffman, *The Conservation of Orbital Symmetry*. Verlag Chemie/Academic Press, New York (1970); (b) R. B. Woodward and R.Hoffman, *Angew. Chem., Int. Ed. Engl.* **8**, 781 (1969).
11. D. F. McMillen and D. M. Golden, *Annu. Rev. Phys. Chem.* **33**, 493 (1982).
12. B. K. Carpenter, *J. Am. Chem. Soc.* **115**, 9806 (1993).
13. C.-Y. Lin, PhD Dissertation, Catholic University o,f America (1986).
14. E. W. Diau, M. C. Lin and C. F. Melius, *J. Chem. Phys.* **101**, 3923 (1994).
15. M. R. Berman and M. C. Lin, *J. Phys. Chem.* **87**, 3933 (1983).
16. D. S. Y. Hsu, W. M. Shaub, T. Creamer, D. Gutman and M. C. Lin, *Ber. Bunsenges. Phys. Chem.* **87**, 909 (1983).
17. J. Troe, *J. Phys. Chem.* **83**, 114 (1979).